JOURNAL OF MATERIALS SCIENCE 13 (1978) 1521–1537

Evaluation of biaxial stress failure surfaces for a glass fabric reinforced polyester resin under static and fatigue loading

M. J. OWEN, J. R. GRIFFITHS*
Department of Mechanical Engineering, University of Nottingham, University Park, Nottingham, UK

In an attempt to evaluate failure theories for a glass fabric reinforced polyester resin over 370 tests have been conducted on thin-walled tubes under combined axial loading and internal pressure, both for static and fatigue loading. For plane stress the results are considered in relation to imaginary failure surfaces in σ_1, σ_2, σ_6 space. A limited measure of agreement between theories and results can be obtained after highly subjective selection of data. Only those theories which involve complex stress properties provide a reasonable fit. The behaviour of tubular specimens is strongly influenced by the presence of joints in the reinforcements.

Nomenclature

σ_x, σ_y	nominal hoop and axial (principal) stresses in a thin-walled tube
$\sigma_1, \sigma_2, \sigma_6$	normal and shear stresses in the direction of the principal material axes
F_1, F_2, F_6	strengths in the principal material directions and the in-plane shear strength
F_{1t}, F_{2t}	tensile strengths in the principal material directions
F_{1c}, F_{2c}	compressive strengths in the principal material directions
K_2	a constant evaluated from a combined stress test
H_{12}	normal stress interaction component of a strength tensor
α	off-axis angle
S–N curve	conventional stress–log life fatigue curve
R	principal stress ratio, σ_y/σ_x

1. Introduction

Owen and Found [1] have reported that it is difficult to discriminate between biaxial stress theories of failure for a glass reinforced plastic by means of off-axis fatigue testing. Furthermore, small differences in the observed strengths make considerable differences to the shape of the proposed failure surfaces for some of the more recent theories [2]. These observations are consistent with those of Schneider [3], Collins and Crane [4], and Wu [5] who reported the same difficulties with static tests on other types of FRP. Owen and Found [6] and Owen *et al.* [7] have reported the use of a multi-station machine for subjecting thin-walled GRP tubes to various combinations of axial load and internal pressure under static and fatigue loading, thereby producing principal stress ratios in the range $R = +1.0$ to $R = -1.0$ in the cylinder walls. This machine has now been used to study the same fabric reinforced polyester resin material previously reported by Owen and Found [1]. Full details of the work have been reported in a thesis by Griffiths [2].

Table I summarizes the better known theories of failure for anisotropic materials specialised for

*Dr Griffiths is now with the Mining Research and Development Establishment, Ashby Road, Stanhope Bretby, Burton-on-Trent, UK.

TABLE I Failure theories

Reference	Key to figs.*	Failure criterion
Group 1		
Maximum stress (Stowell and Liu [8])	A	$\sigma_1 = F_1;\quad \sigma_2 = F_2;\quad \sigma_6 = F_6$
Maximum strain (Waddoups [9])		$\sigma_1 = F_1 + \nu_{12}\sigma_2;\quad \sigma_2 = F_2 + \nu_{12}\dfrac{E_{22}}{E_{11}}\sigma_1;\quad \sigma_6 = F_6$
Hill [10]	B	$\left(\dfrac{\sigma_1}{F_1}\right)^2 - \left(\dfrac{1}{F_1^2} + \dfrac{1}{F_2^2} - \dfrac{1}{F_3^2}\right)\sigma_1\sigma_2 + \left(\dfrac{\sigma_2}{F_2}\right)^2 + \left(\dfrac{\sigma_6}{F_6}\right)^2 = 1$
Azzi and Tsai [11]	B	$\left(\dfrac{\sigma_1}{F_1}\right)^2 - \dfrac{\sigma_1\sigma_2}{F_1^2} + \left(\dfrac{\sigma_2}{F_2}\right)^2 + \left(\dfrac{\sigma_6}{F_6}\right)^2 = 1$
Norris interaction (Norris and McKinnon [12])	C	$\left(\dfrac{\sigma_1}{F_1}\right)^2 + \left(\dfrac{\sigma_2}{F_2}\right)^2 + \left(\dfrac{\sigma_6}{F_6}\right)^2 = 1$
Norris failure (Norris [13])	D	$\left(\dfrac{\sigma_1}{F_1}\right)^2 - \dfrac{\sigma_1\sigma_2}{F_1F_2} + \left(\dfrac{\sigma_2}{F_2}\right)^2 + \left(\dfrac{\sigma_6}{F_6}\right)^2 = 1;\quad \left(\dfrac{\sigma_1}{F_1}\right)^2 = 1;\quad \left(\dfrac{\sigma_2}{F_2}\right)^2 = 1$
Hoffman [14]	E	$\dfrac{\sigma_1^2 - \sigma_1\sigma_2}{F_{1c}F_{1t}} + \dfrac{\sigma_2^2}{F_{2c}F_{2t}} + \left(\dfrac{F_{1c} - F_{1t}}{F_{1c}F_{1t}}\right)\sigma_1 + \left(\dfrac{F_{2c} - F_{2t}}{F_{2c}F_{2t}}\right)\sigma_2 + \left(\dfrac{\sigma_6}{F_6}\right)^2 = 1$
Group 2		
Modified Marin (Franklin [15])	F	$\dfrac{\sigma_1^2 - K_2\sigma_1\sigma_2}{F_{1c}F_{1t}} + \dfrac{\sigma_2^2}{F_{2c}F_{2t}} + \left(\dfrac{F_{1c} - F_{1t}}{F_{1c}F_{1t}}\right)\sigma_1 + \left(\dfrac{F_{2c} - F_{2t}}{F_{2c}F_{2t}}\right)\sigma_2 + \left(\dfrac{\sigma_6}{F_6}\right)^2 = 1$
Goldenblat and Kopnov [16]	G	$\frac{1}{2}\left(\dfrac{1}{F_{1t}} - \dfrac{1}{F_{1c}}\right)\sigma_1 + \frac{1}{2}\left(\dfrac{1}{F_{2t}} - \dfrac{1}{F_{2c}}\right)\sigma_2 + \left[\frac{1}{4}\left(\dfrac{1}{F_{1t}} + \dfrac{1}{F_{1c}}\right)^2\sigma_1^2 + \frac{1}{4}\left(\dfrac{1}{F_{2t}} + \dfrac{1}{F_{2c}}\right)^2\sigma_2^2 + 2H_{12}\sigma_1\sigma_2 + \left(\dfrac{\sigma_6}{F_6}\right)^2\right]^{1/2} = 1$
Tsai and Wu [17]	H	$\left(\dfrac{1}{F_{1t}} - \dfrac{1}{F_{1c}}\right)\sigma_1 + \left(\dfrac{1}{F_{2t}} - \dfrac{1}{F_{2c}}\right)\sigma_2 + \dfrac{\sigma_1^2}{F_{1t}F_{1c}} + \dfrac{\sigma_2^2}{F_{2t}F_{2c}} + 2H_{12}\sigma_1\sigma_2 + \left(\dfrac{\sigma_6}{F_6}\right)^2 = 1$ and $\dfrac{1}{F_{1t}F_{1c}} \cdot \dfrac{1}{F_{2t}F_{2c}} - H_{12}^2 \geqslant 0$ for stability

*A, B etc. are the key letters to figures

plane stress conditions. These theories can be represented as failure surfaces by plotting the in-plane stresses σ_1, σ_2, and σ_6 in Cartesian space [4, 18]. The origin of the stress space should lie within the failure surface and it is generally agreed that the surface should be closed. The surfaces which represent the Group 2 theories in Table I can be open unless the adjustable constant or normal stress-interaction term in the tensor theories lies between certain values. For this reason Tsai and Wu [17] have included a stability criterion. The validity of the failure surfaces is tested exper-

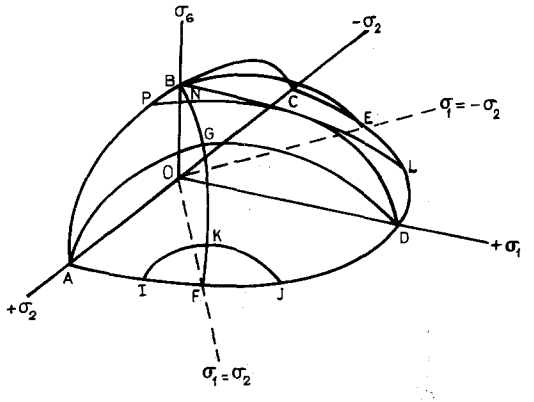

Figure 1 Failure surface in σ_1, σ_2, σ_6 space.

imentally by comparing the stresses at failure under biaxial stress conditions with corresponding points on the failure surfaces. Fig. 1 shows part of a hypothetical failure surface represented in σ_1, σ_2, σ_6 space, where for illustrative convenience the axes form a left-handed coordinate system. The surface is expected to be symmetrical about the $\sigma_6 = 0$ plane since the positive and negative shear conventions only amount to viewing the material from opposite sides. Furthermore for this material $F_{1t} = F_{2t}$ and $F_{1c} = F_{2c}$ and hence the $\sigma_1 = \sigma_2$, σ_6 plane is a plane of symmetry. Although $F_{1t} \simeq F_{1c}$ the off-axis tensile and compressive behaviour are not entirely symmetrical and hence the $\sigma_1 = -\sigma_2$, σ_6 plane is not a plane of symmetry [1].

The principal (axial and hoop) stresses σ_x and σ_y in a thin-walled tube or σ_x in an off-axis uniaxial loading test can be transformed to the principal material axes using the usual relationships. For tubes with $\alpha = 0^\circ$, $\sigma_6 = 0$ and varying the stress ratio R from $+1$ to -1 produces results which define the boundary FJDLE. For tubes with $\alpha = 45^\circ$, $\sigma_1 = \sigma_2$ and as R changes from $+1$ to -1 results can be produced which define the curve FB. For $R = -1$ varying α from 0° to 45° produces results which define the curve EB. The curves FJDLE, FB, and EB lie in plane sections of the failure surface and because of the expected symmetries provide a reasonable definition of the failure surface. Other test conditions produce results which lie along general curves on the surface. Off-axis tensile tests or tests on tubes at $R = 0$ produce results along DG as α changes from 0° to 45° reflecting into AG by symmetry. It is results along this line which fail to discriminate between failure theories [3, 19] or lead to the definition of unacceptable surfaces [1]. As α varies from 0° to 45°, $R = -0.5$ gives the curve LN and $R = +0.5$ gives the curve JK. $R = +0.5$ is the condition for a closed ended thin-walled tube subject to internal pressure. Clearly only a small part of the failure surface can be examined by this test condition. Finally, $R = 1$ gives the invariant point F as α is changed.

In principle the determination of the failure surface requires only the determination of the principal material strengths and for the Group 2 theories the results of a single complex stress test. Intuitively failure surfaces representing the onset of damage or fatigue failure would be expected to lie inside the failure surfaces representing short term static rupture. In practice there is scatter in strength properties and failure cannot be represented by a unique surface. Furthermore as Owen and Found [1] pointed out the shapes of the surfaces which represent the Group 2 theories are very sensitive to the values used. The predicted surfaces are often intuitively unacceptable either because they are open-ended, or because they appear to intersect.

The work reported in the present paper represents part of a continuing attempt to evaluate the biaxial stress behaviour of a typical glass reinforced plastic under short term static loading and fatigue loading taking into account both the onset of matrix cracking and rupture of the material.

2. Equipment and methods of testing

Fig. 2 shows the multi-station rig for applying combined axial loading and internal pressure to thin-walled tubes. From left to right there is a loading frame arranged for static testing using a hand operated pump, a control console with XY recorders, two loading frames for fatigue tests, a hydraulic pulsator pump, and two further fatigue loading frames. Fig. 3 shows a loading frame diagrammatically. Two substantial end plates are separated by four columns to provide a stiff frame. Within the frame in a single chain are the axial load cell, axial load ram, and the specimen with end caps and loading bars. Oil is supplied to the system via the loading ram and hence through a small diameter hole in the lower loading bar to the interior of the specimen. Air can be released through the centre of the upper loading bar. Since the same supply of oil (Shell Tellus 15 mineral oil) is used for the ram and the cylinder, the principal stresses in the cylinder are always in

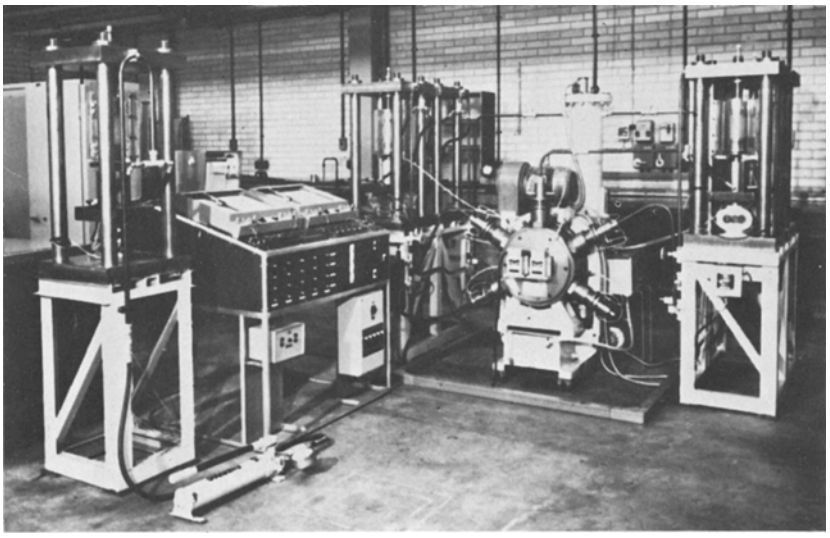

Figure 2 The testing machine.

phase. In order to vary the principal stress ratio it is necessary to have a set of nine interchangeable rams of different diameters. With the multi-station machine and careful planning of the test programme no great inconvenience is occasioned by this method. In practice there is some friction at the loading ram and both the axial load and the pressure are monitored. Under fatigue loading conditions the ram friction is low enough to permit rotation of the pistons to accommodate the torsional displacements which occur in cylinders with off-axis reinforcements. For static tests the oil is supplied by means of a hand-operated pump and for fatigue tests by the pulsator pump. The latter has been fully described by Owen [20]. The pulsator has five cylinders with pistons driven by a common eccentric. The cylinders are hydraulically independent so that they can be adjusted separately and there is one cylinder for each loading frame. By moving a cylinder in or out relative to the eccentric the piston closes the inlet ports earlier or later in the stroke. Once the ports are closed a pre-determined amount of oil is forced into a closed elastic system consisting of the specimen, the ram, and the associated pipework. The maximum working pressure is 13.8 $MN\,m^{-2}$. Almost all of the elastic work is recovered in each stroke and so power consumption and heating effects in the oil are very small. Small amounts of leakage are automatically made up by a low pressure supply each time the inlet ports are uncovered. The pulsator has a variable speed drive covering the range 55 to 330 cycles min^{-1} and is normally used at 100 cycles min^{-1}. The hydraulic circuit for each frame includes a solenoid-operated dumping valve and a pressure-operated switch which controls the cycle counter. A comprehensive description of the machine has been given by Found [21].

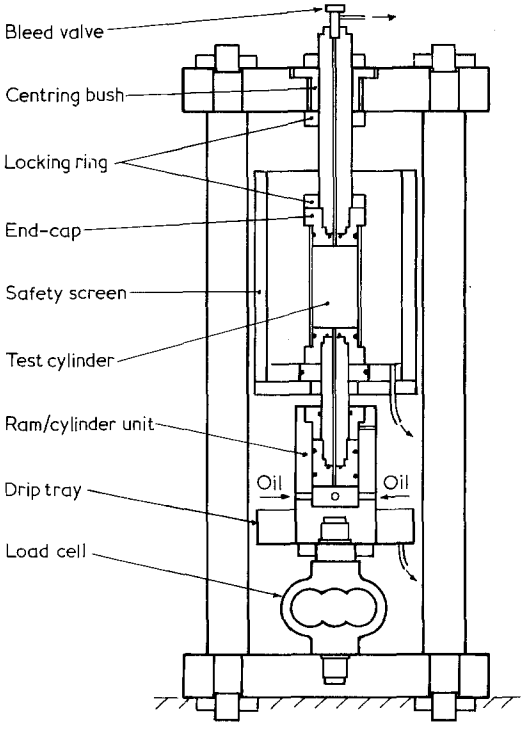

Figure 3 The loading frame.

A few in-plane shear fatigue results were obtained by testing thin-walled tubes in a constant deflection torsional machine driven by a variable throw eccentric. The specimen was connected through end caps similar to those used in the

hydraulic machine in tandem with a strain gauged torsion bar. Torque was applied to the assembly at 100 cycles min^{-1} through ball contacts arranged to prevent the transmission of a bending moment.

A considerable amount of supplementary fatigue testing was carried out on flat laminate specimens subjected to axial loading in addition to that reported by Owen and Found [1]. These tests were conducted in the axial loading fatigue machines previously described by Owen [20]. Five loading frames are available and can apply any combination of mean and alternating load within the extreme limits of ± 6000 lbf. They are driven by a pulsator pump almost identical with the one described above. As far as is possible for FRP the test methods were in accordance with BS 3518 "Methods of Fatigue Testing". Owen [22] has provided a commentary on the relevance of this standard for FRP.

3. Materials and specimen preparation

Details of the materials used are summarized in Table II. The procedure for making thin-walled tubes was as follows. A 65 mm diameter mandrel was wrapped with a single layer of "Melinex" release film. Sections of fabric were cut from the roll of sufficient length to give five turns around the mandrel plus a 40 mm circumferential overlap. The width of the fabric was sufficient for each tube to provide two specimens. Previous work confirmed that flat laminates have equal strengths in the warp and weft directions of the fabric [1]. It was just possible to cut a sufficient length of fabric at 45° to the reinforcement to make a single five-turn tube. After cutting the fabric it was soaked in a bath of prepared resin until the fibres were fully wetted

TABLE II Materials

Reinforcement type	Lay-up	Thickness (mm)	Glass content (wt %)
Tyglass Y449 E-glass fabric T5 finish	5 layers	2.08	52.3
Polyester resin – Beetle L2615 BIP Chemicals Ltd.			
Maleic anhydride		1 mol	
Phthalic anhydride		1 mol	
Propylene glycol		3 mol	
Alkyd/styrene ratio		65/35	
Hydroquinone		0.008% on blended resin	
Catalyst MEKP		1%	
Accelerator Cobalt napthenate		½%	
Room temperature cure		18 h	
Postcure		3 h at 80° C	

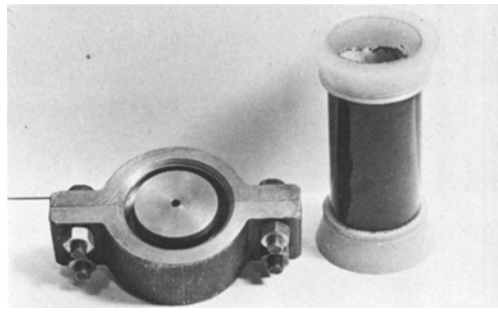

Figure 4 Specimen and end-cap for tensile axial load.

and as much air as possible had been dispersed. The leading edge of the fabric was then placed on the mandrel and wrapped onto the slowly rotating mandrel whilst rolling out surplus resin. On completion the outer surface was covered with a further layer of "Melinex" release film and the mandrel left slowly turning in light contact with a roller until gelling of the resin occurred. This method produced void-free tubes of uniform thickness and hence uniform glass content. Considerable care was required at all stages to avoid disturbing the reinforcement pattern.

Tubes intended for testing with compressive axial loads were subsequently overwound with additional fabric and resin to thicken the ends. After post-curing the specimens were cut to length and prepared for testing. Fig. 4 is a photograph of an end-cap and a specimen prepared for tensile testing. The end-cap provides an internal steel plug which is a sliding fit inside the specimen and houses an "O" ring to provide a hydraulic seal. The specimen is placed over the plug and then cast in place with epoxy casting resin so that a wedge-section ring is formed. This has been found satisfactory for all static and fatigue loading. The end-caps for compressive loading provide the internal plug and seal but simply bear on to the thickened ends of the specimen. Torsion specimens were prepared in a similar manner to tension specimens but the cast ends incorporated lugs to transmit the torque. All the specimens were 65 mm internal diameter with 1.95 mm wall thickness. For compressive axial loads the length was 180 mm with 40 mm overwound at each end leaving 100 mm gauge length. The tensile end-caps left a gauge length of 120 mm and the torsional end-caps left a length of 60 mm.

Silicone rubber liners were used to prevent oil under pressure from being forced into the material

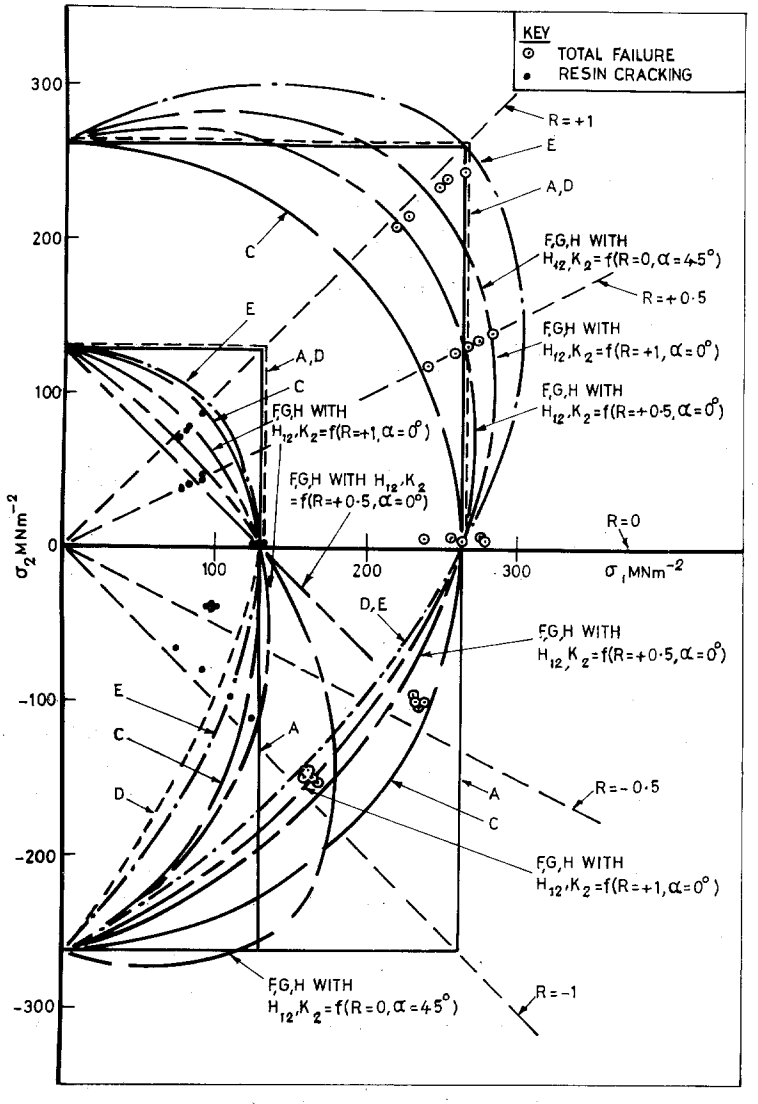

Figure 5 Static results for tubes with $\alpha = 0°$ and R taking values from +1 to −1 (corresponding to curve FJDLE in Fig. 1). For key to curves see Table I.

after the advent of damage and to reduce seepage from specimens tested to rupture. The tubes were cleaned with acetone and treated with ICI Primer OP before being coated with ICI Silcoset 105 cold-curing silicone rubber with added carbon black to provide a darkened background for viewing damage. The carbon black made the liners porous and a second layer of unfilled rubber was applied. However the ICI Primer made the liners very difficult to remove (for glass content determination) and Midland Silicones MS 2650 primer was used for static work to make liner removal easier.

Flat specimens required for supplementary tests were prepared by the methods described by Owen and Found [1].

4. Static results

In order to examine the failure theories of Table I results were obtained from tubes subjected to monotonically increasing pressure noting the onset of resin cracking as well as rupture. In some cases separate tests were conducted to determine the onset of resin cracking. The tests conducted were

(a) at $\alpha = 0°$ with R varying from +1 to −1,

(b) at $\alpha = 45°$ with R varying from +1 to −1,

and (c) at $R = -1$ with α varying from 0° to 45°, giving results corresponding to curves FJDLE, FB, and EB respectively on the failure surface of Fig. 1. However they were slightly displaced from the nominal positions on the failure surface due to ram friction.

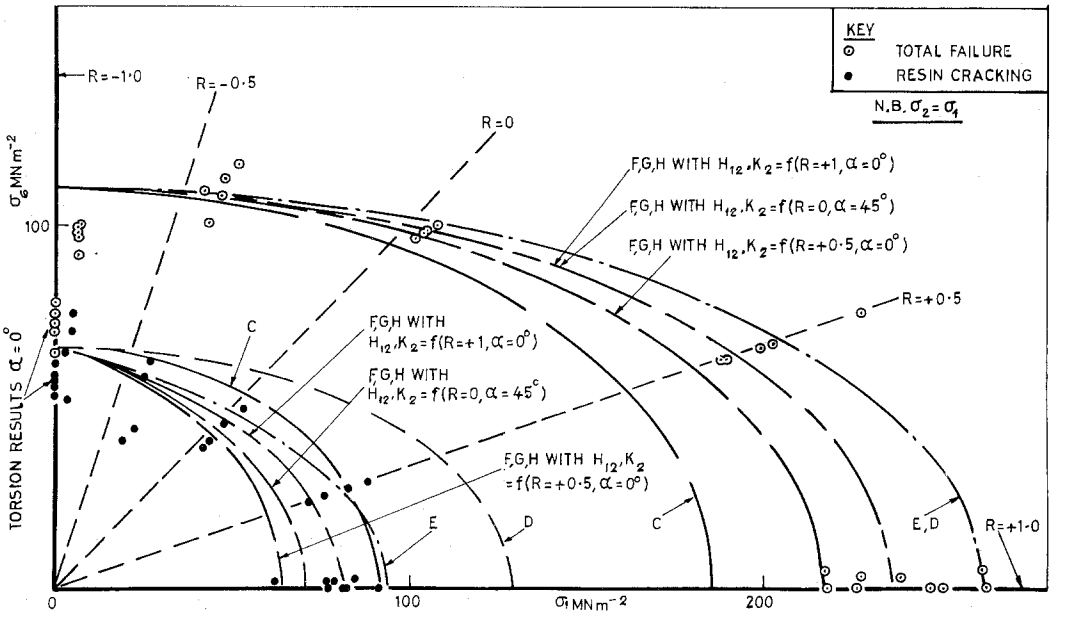

Figure 6 Static results for tubes with $\alpha = 45°$ and R taking values from +1 to −1 (corresponding to curve FB in Fig. 1). For key to curves see Table I.

Fig. 5 presents the results of 45 tests at $\alpha = 0°$ showing the onset of resin cracking and rupture for R varying from +1 to −1. Broken lines radiating from the origin correspond to the nominal R values and ram friction produces the offset of the results from these lines. Fig. 6 shows a further 45 results based on $\alpha = 45°$ tubes with R varying from +1 to −1. The results are plotted in terms of σ_6 and σ_1 $(= \sigma_2)$. The $R = +1$ condition is invariant and the results for $\alpha = 0°$ are included for comparison. Although they are slightly offset because of ram friction the agreement is excellent. The $R = -1$, $\alpha = 45°$ condition corresponds to pure torsion on a tube with $\alpha = 0°$. The torsion test results are plotted on the σ_6 axis. Comparison of the torsion test results (Figs. 6 and 7) with the R

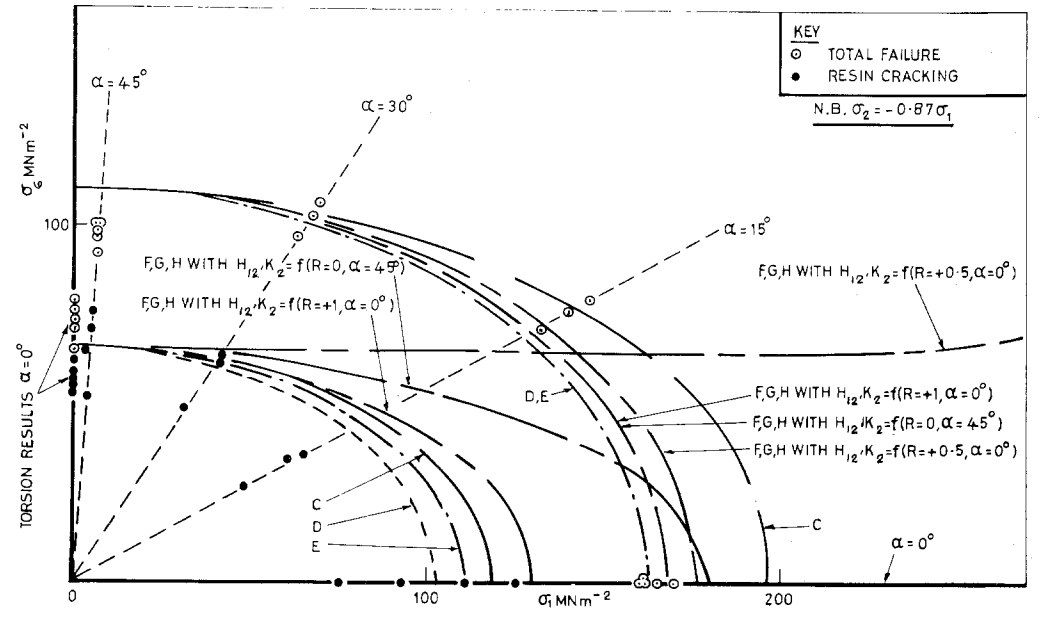

Figure 7 Static results for tubes with $\alpha = 0°$, 15°, 30° and 45° for $R = -1$ (corresponding to curve FE in Fig. 1). For key to curves see Table I.

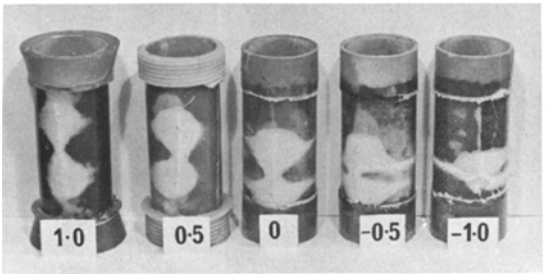

Figure 8 Failed tubes, static loading with $\alpha = 0°$ and R values as indicated.

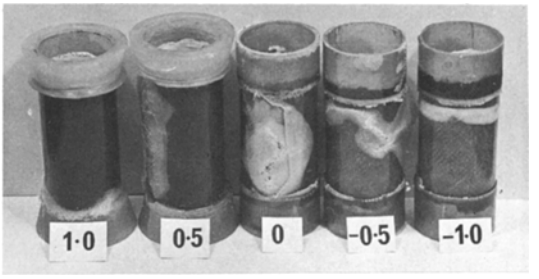

Figure 9 Failed tubes, static loading with $\alpha = 45°$ and R values as indicated.

$= -1$ and $R = -0.5$ (corrected to $R = -0.87$ and $R = -0.41$) results indicates unusual behaviour in this region. Fig. 7 presents results for $R = -1$ (corrected to $R = -0.87$) as α varies from 0° to 45°. Only the 12 results for $\alpha = 15°$ and $\alpha = 30°$ are new since the $\alpha = 0°$ and $\alpha = 45°$ were included in Figs. 5 and 6.

Typical biaxial stress static failures of tubes are shown in Figs. 8 and 9 for $\alpha = 0°$ and $\alpha = 45°$ respectively. In Fig. 9 part of the outer reinforcement layer of the $R = 0$ tube has been removed to show the fracture path more clearly.

5. Discussion of static results

The principal strengths (F_{1t}, F_{1c}, F_{2t}, F_{2c} and F_6) are required in the application of the failure theories. Only F_{1t} (at $R = 0, \alpha = 0°$) and F_6 (at $R = -1$ and $\alpha = 45°$) can be conveniently determined in the test rig because of buckling or gripping problems. F_6 can also be determined from torsion tests. Table III(a) shows values for F_{1t} and F_{1c} obtained from flat laminates. Material symmetry implies $F_{2t} = F_{1t}$ and $F_{2c} = F_{1c}$. Table III(a) highlights a major problem in the interpretation of data and the use of failure theories. There are marked differences between the strength of tubes at $R = 0$ and flat laminates in tension and between different batches of nominally identical materials. These problems have not been satisfactorily resolved although it is believed that, in spite of the presence of an overlap due to bonding, the tubes are stronger because of the absence of edge effects. Eventually it had to be assumed that for the tubes $F_{1t} = F_{2t}$ from material symmetry, and that $F_{1t} = F_{1c}$ and $F_{2t} = F_{2c}$ as observed in the flat laminates. The hoop strength of the $R = 0$, $\alpha = 0°$ tubes was used for F_{1t}.

The Group 2 theories of Table I require complex stress data to evaluate the interaction coefficients K_2 and H_{12} which determine the length and inclination of the failure ellipse in the σ_1, σ_2 plane. Wu [5] has shown that optimum stress ratios exist for any given material. However exceptionally versatile test equipment would be

TABLE III (a) Static principal strengths

Strength	Flat laminates				Tubes	
	Resin cracking strength ($MN\,m^{-2}$)		Rupture strength ($MN\,m^{-2}$)		Resin cracking strength ($MN\,m^{-2}$)	Rupture strength ($MN\,m^{-2}$)
	A	B	A	B		
F_{1t}	83.5	72.8	231.0	209.2	129.1	262.2
F_{2t}	83.5		231.0		129.1	262.2
F_{1c}	191.0		227.0		262.2	262.2
F_{2c}	191.0		227.0		262.2	262.2
F_6	72.5	57.6	72.5	72.3	66.08	110.0*

The tube strengths shown are those used for failure theory prediction.
A Owen and Found (1975); 7-layered laminates, 58 wt % glass.
B Present paper; 5-layered laminates, 52 wt % glass.
*Assumed value of F_6 based on general data trend.

TABLE III (b) Fatigue principal strengths (tubes) for failure theory prediction at 10^6 cycles

Strength	Resin cracking strength ($MN\,m^{-2}$)	Rupture strength ($MN\,m^{-2}$)
F_{1t}	15.74	66.16
F_{2t}	15.74	66.16
F_{1c}	36.20	70.99
F_{2c}	36.20	70.99
F_6	10.14	28.10

necessary to obtain these ratios experimentally. For the present material using the Nottingham rig the optimum condition obtainable is $R = 1$, $\alpha = 0^\circ$. Predictions have been made based on H_{12} obtained from this condition. For comparison purposes predictions have also been made with H_{12} determined for $R = +0.5$, $\alpha = 0^\circ$ and $R = 0$, $\alpha = 45^\circ$, corresponding to a closed end tube under internal pressure and a 45° off-axis flat specimen respectively. These latter conditions are more readily obtained and might be used in the absence of specialized test equipment.

There is a further difficulty in determining the in-plane shear strength F_6 for use with the failure theories. Figs. 6 and 7 include results from torsion tests ($\alpha = 0^\circ$) and internal pressure tests ($\alpha = 45^\circ$, $R = -1$, corrected to $R = -0.87$ approximately). It was found that the torsional strength varied with length (shorter cylinders being stronger) and that collapse was almost coincident with the onset of damage. Comparison of the torsion results with adjacent conditions in Figs. 6 and 7 shows consistency for the onset of resin cracking, but not for rupture. It was concluded that torsion (and the $R = -0.87$ $\alpha = 45^\circ$ condition) produces a premature type of failure possibly influenced by buckling. After careful consideration of the results it was assumed that at rupture $F_6 = 110\,MN\,m^{-2}$ would be an appropriate value for use with the failure theories. If this is not done then a continuous failure surface describing all the observed data would give different results for positive and negative shear. This is impossible for a symmetrical material of this type. Further support for this procedure was also found in the fatigue data and will be noted later.

Figs. 5 to 7 show that the Group 2 type theories provide the most accurate prediction of the observed rupture behaviour. All Group 2 theories produce almost identical results for a material of this type. The constants H_{12} and K_2 derived from $R = +1$, $\alpha = 0^\circ$ data and $R = 0$, $\alpha = 45^\circ$ data were virtually identical and hence so are the predicted curves. The curve based on $R = +0.5$ $\alpha = 0^\circ$ data is more conservative in the first quadrant of Fig. 5 but provides a good basis for design. Of the Group 1 theories the Norris failure [13] theory provides a most acceptable prediction and is thus useful when complex stress data is not available.

For resin cracking the picture is not so clear because the $R = 0$, $\alpha = 0^\circ$ data does not correlate satisfactorily with the rest and since this is used as a principal material strength anomalies here are bound to affect the predictions adversely. Thus none of the predictions are generally acceptable but the most useful are the Group 2 theories based on $R = +1$, $\alpha = 0^\circ$ data and, the Hoffman [14] and Norris Interaction [12] theories of Group 1. The Group 2 theory prediction based on $R = +0.5$, $\alpha = 0^\circ$ data is an open ended hyperbolic surface. The Tsai and Wu theory is strictly invalid under these circumstances since the magnitude of H_{12} violates the imposed stability criterion shown in Table I.

6. Fatigue results

It was not practicable to cover all the conditions of the static programme because of the large number of specimens required. Referring to Fig. 1, tests were designed to explore curve FJDLE ($\alpha = 0^\circ$, $\sigma_6 = 0$) and curve FB ($\alpha = 45^\circ$, $\sigma_1 = \sigma_2$). Five biaxial stress ratios were used both for $\alpha = 0^\circ$ and $\alpha = 45^\circ$, with separate specimens for resin cracking and rupture. A few torsion tests with $\alpha = 0^\circ$ were conducted. Flat laminate (uniaxial) test results were also obtained with $\alpha = 0^\circ$ and $\alpha = 45^\circ$ for comparison with tube test results.

Fig. 10 shows results for flat laminate specimens at the onset of resin cracking and rupture. In this and in other figures static results are represented by a vertical bar at 0.25 cycle, where the length of the bar indicates the observed scatter and the mean value is marked on the bar. The fatigue curves are first or second order regression lines. Fig. 10 includes results for specimens containing an overlap joint simulating wound tubes.

The results of 256 fatigue tests on tubes are summarized in Figs. 11 to 14. Full details have been given by Griffiths [2]. Fig. 11 shows a typical sample of the results compared with flat laminate results from Fig. 10. Also included are $R = -1$,

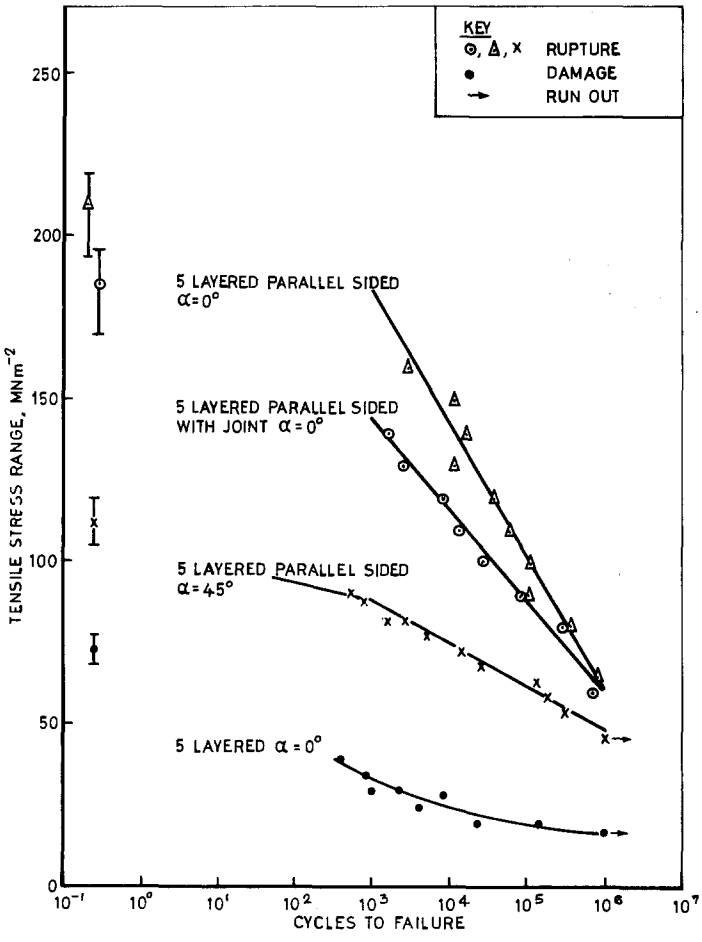

Figure 10 Fatigue curves for flat laminate specimens, axial tensile loading zero to maximum stress.

$\alpha = 45^\circ$ results presented in terms of maximum shear stress for comparison with torsion results for $\alpha = 0^\circ$ tubes. Figs. 12 to 14 compare the fitted curves for all the tube tests with $\alpha = 0^\circ$ and $\alpha = 45^\circ$. Results were not obtained for $R = 1$, $\alpha = 45^\circ$ because of testing difficulties. The rupture results are cross-plotted as constant life diagrams in Figs. 15 and 16. Figs. 15 and 16 are plotted in terms of hoop σ_x and axial stress σ_y so that in Fig. 15 where $\alpha = 0^\circ$, $\sigma_x = \sigma_1$, σ_2 and $\sigma_6 = 0$. However in Fig. 16, σ_6 differs with each stress ratio and $\sigma_x \neq \sigma_1$, $\sigma_y \neq \sigma_2$. For $R = +1$, $\alpha = 0^\circ$ results were used because this is an invariant condition. Figs. 17 and 18 show rupture results at 10^6 cycles compared with predicted behaviour based on failure theories. Figs. 19 and 20 are similar figures for resin cracking.

7. Discussion of fatigue results

The wrapped tubes inevitably have an overlap type of joint in the reinforcement running along the length of the tube. It has been shown that reinforcement joints have a dominant effect on the fatigue properties of chopped strand mat reinforced tubes [2, 7]. Fig. 10 includes fatigue results for simulated lap joints in flat laminates. It appears that the joint effect is significant at short lives but becomes negligible at 10^6 cycles. In Fig. 11 it can be seen that these results closely represent the behaviour of $R = 0$, $\alpha = 0^\circ$ tubes. Examination of failed tubular or flat specimens shows that the overlap region delaminates at high stresses precipitating complete failure. At lower fatigue stresses this behaviour is not observed. Fig. 11 also shows that tubes ($R = 0$, $\alpha = 45^\circ$) are stronger than flat specimens ($\alpha = 45^\circ$). This is consistent with previous observations [23, 24]. Fig. 11 also includes a comparison of torsion ($\alpha = 0^\circ$) results with $R = -1$, $\alpha = 45^\circ$ results. These two conditions are theoretically equivalent and the results are most consistent at the longer lives (lower stresses). It is believed that at the lower stresses the torsion specimens are free from premature failure after the onset of damage. Fig. 12 compares the $\alpha = 0^\circ$ and $\alpha = 45^\circ$ results and illustrates the

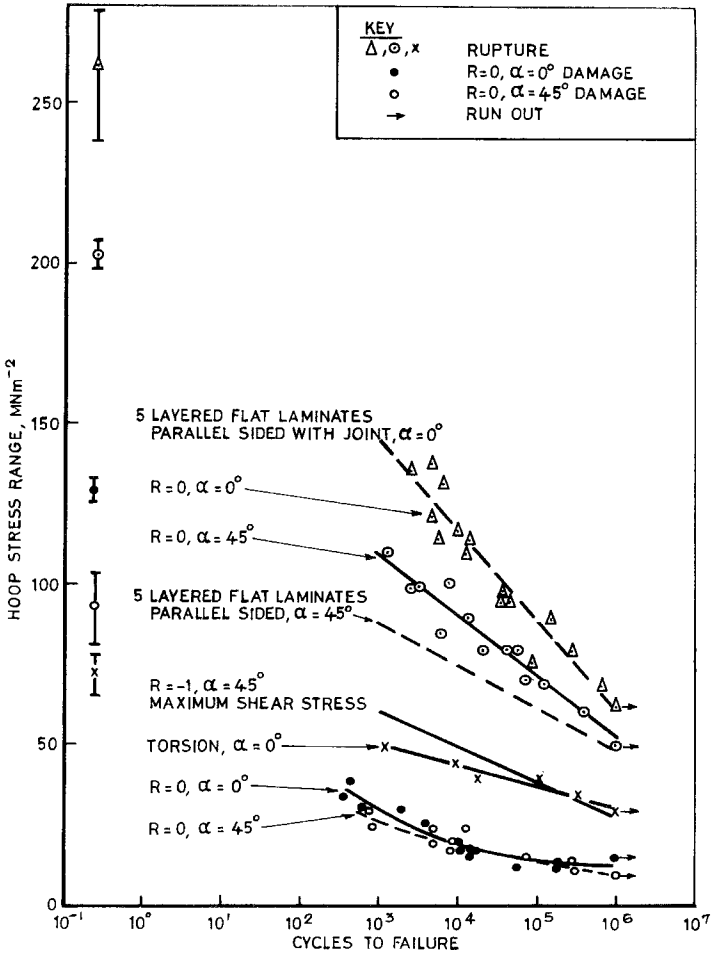

Figure 11 Typical fatigue results for tubes (data points shown) compared with flat laminate results reproduced from Fig. 10 (no data points shown).

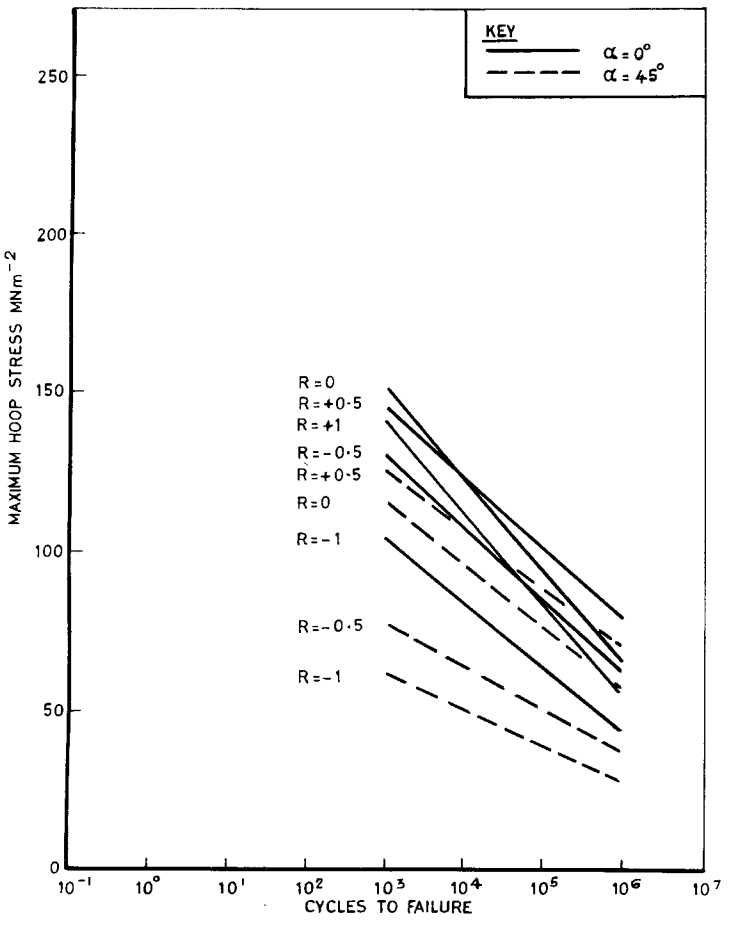

Figure 12 Comparison of fatigue results for tubes at rupture.

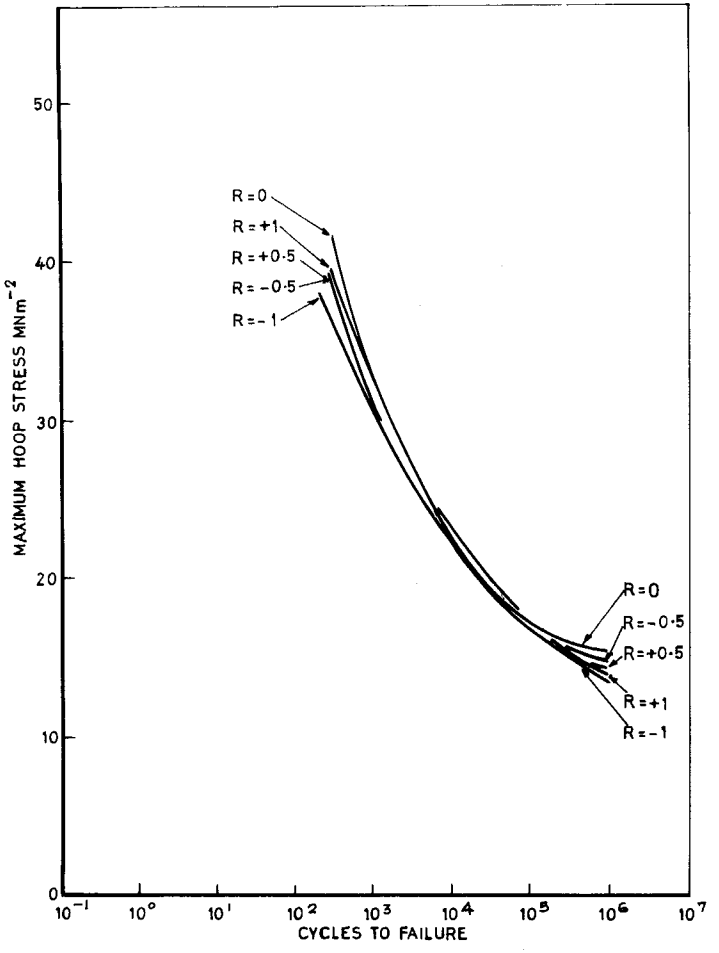

Figure 13 Comparison of fatigue results for tubes at onset of damage ($\alpha = 0°$).

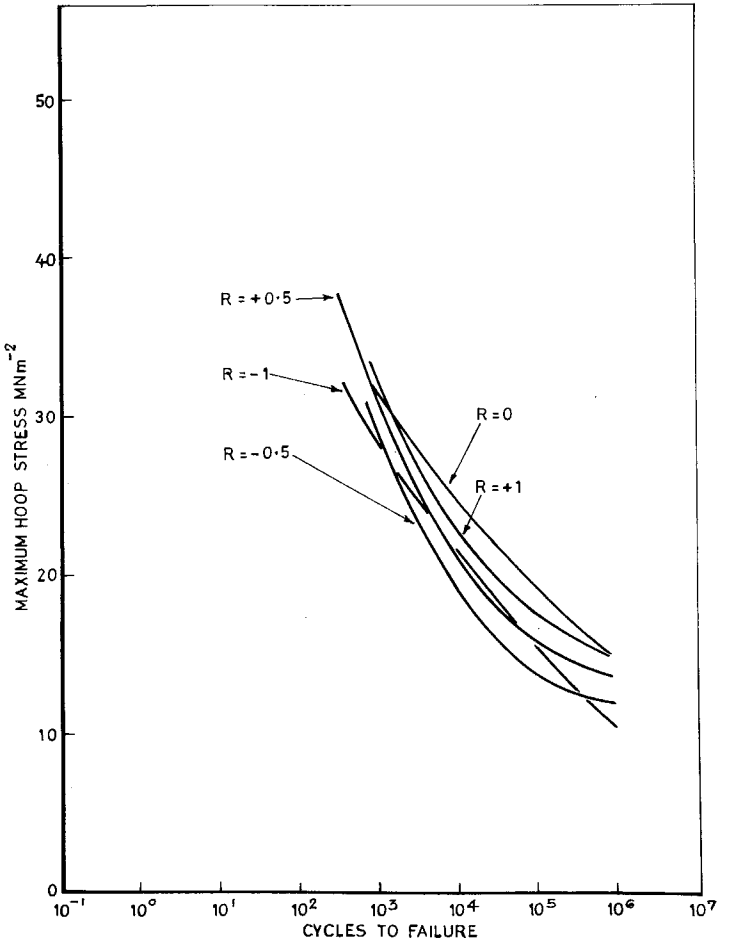

Figure 14 Comparison of fatigue results for tubes at onset of damage ($\alpha = 45°$).

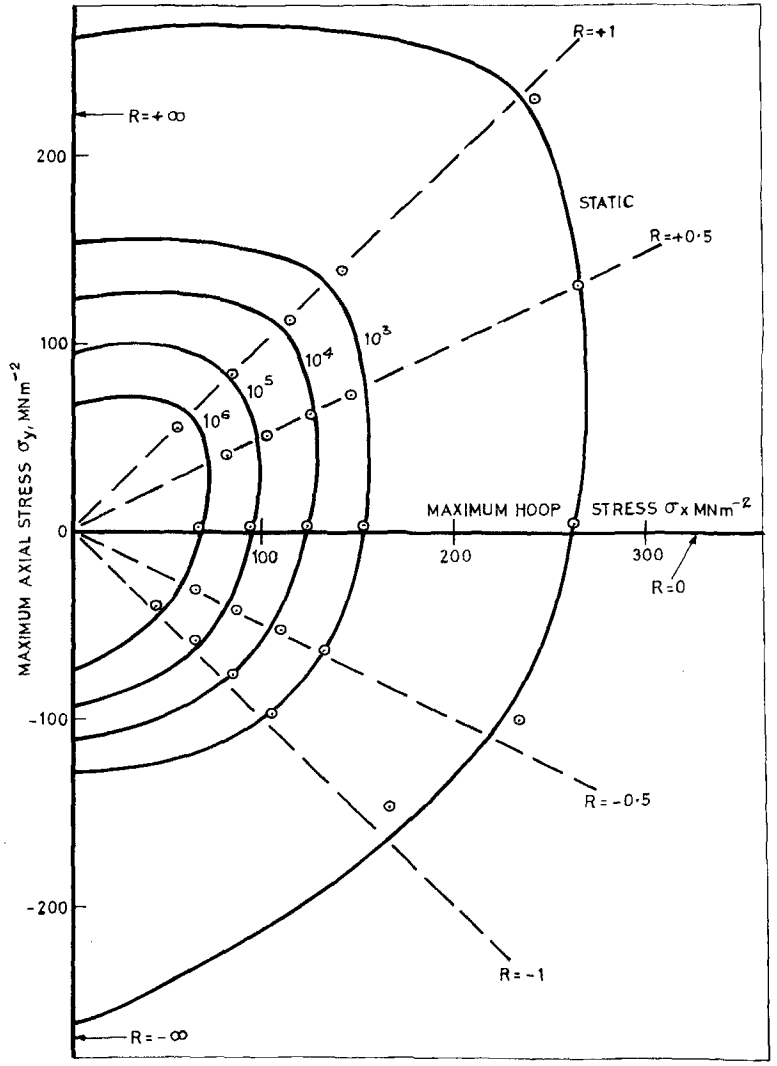

Figure 15 Fatigue results for rupture of tubes presented as constant life diagrams ($\alpha = 0°$).

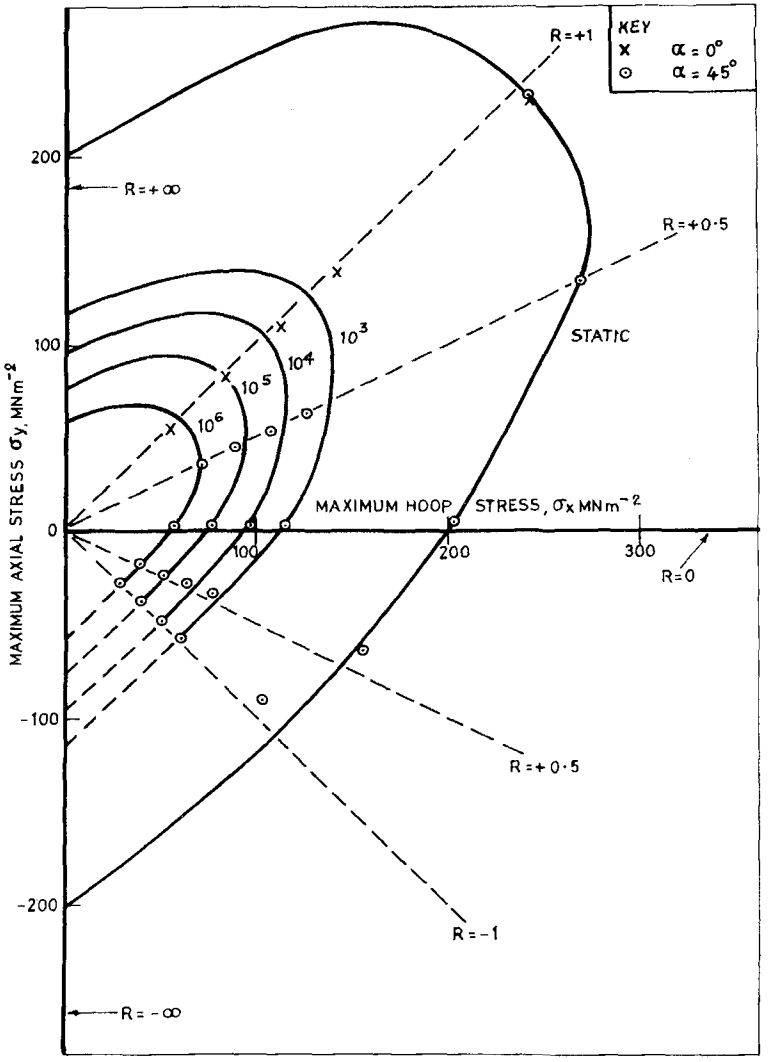

Figure 16 Fatigue results for rupture of tubes presented as constant life diagrams ($\alpha = 45°$).

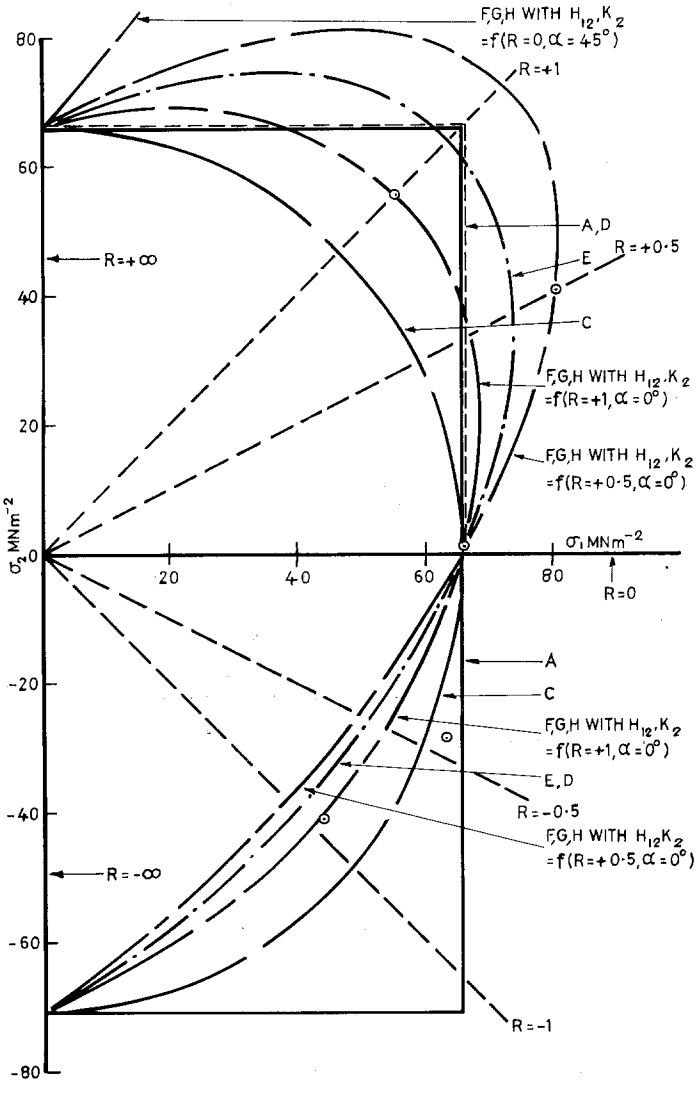

Figure 17 Fatigue results for rupture of tubes in 10^6 cycles compared with the failure theories of Table I (see Table I for key to curves). R takes the values -1 to $+1$ and $\alpha = 0°$ corresponding to curve FJDLE in Fig. 1.

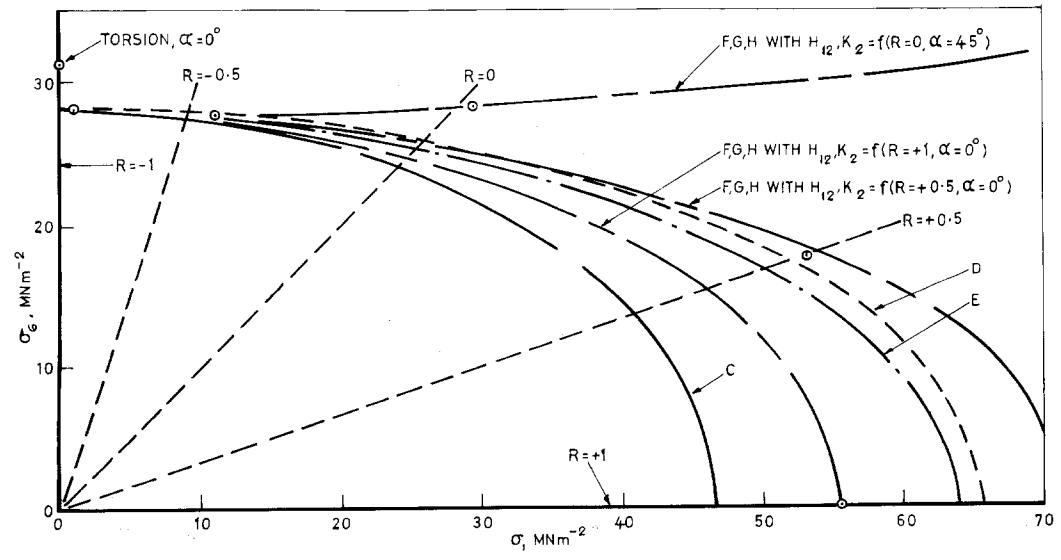

Figure 18 Fatigue results for the rupture of tubes in 10^6 cycles compared with the failure theories of Table I (see Table I for key to curves). R takes values from $+1$ to -1 with $\alpha = 45°$ corresponding to curve FB in Fig. 1.

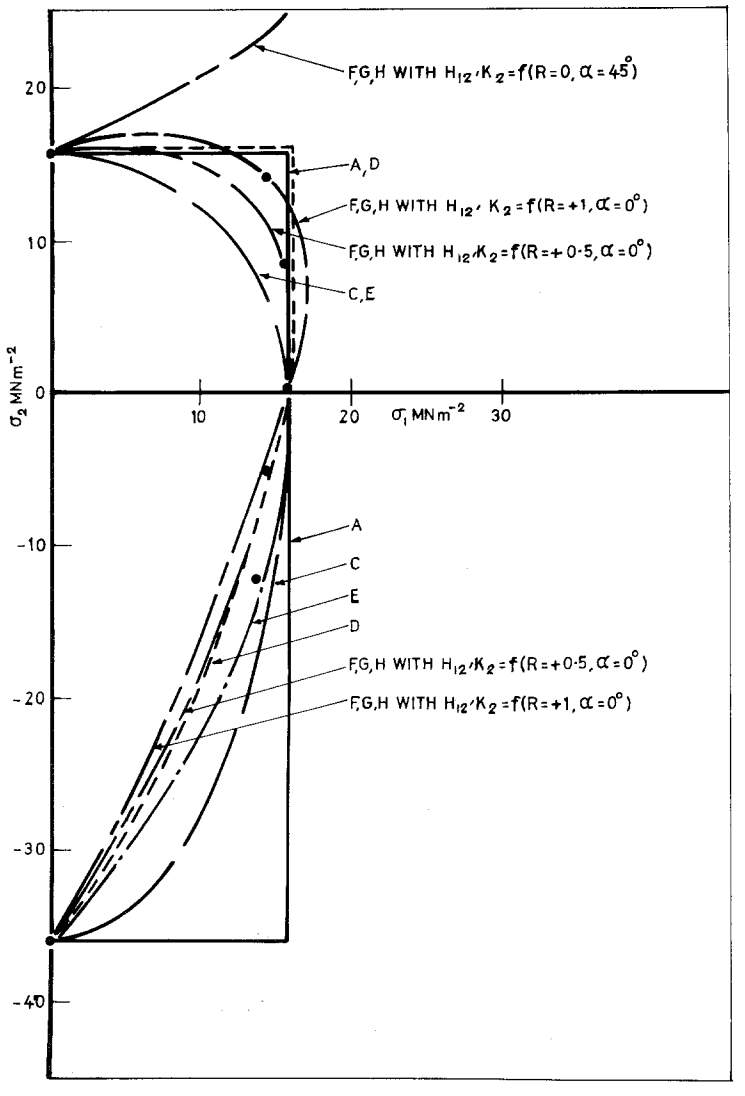

Figure 19 Fatigue results for the onset of damage in tubes at 10^6 cycles compared with the failure theories of Table I (see Table I for key to curves). R takes values from $+1$ to -1 with $\alpha = 0^\circ$ corresponding to curve FJDLE in Fig. 1.

marked effect that the in-plane shear stress has on strength.

Fig. 13 shows that the resin cracking behaviour in $\alpha = 0^\circ$ tubes is controlled by tensile stress (hoop stress) and that at 10^6 cycles resin cracking occurs at only 6% approximately of the principal tensile strength. There is slightly greater variability in Fig. 14 ($\alpha = 45^\circ$). A comprehensive report of damage mechanisms would make the present paper excessively long. However factors found to influence the cracking behaviour were joints, (at all R except $R = +1.0$) and voids. The onset of damage in Figs. 13 and 14 was judged for void free regions. Voids appeared to have a fatigue strength reduction factor of 1.3 to 1.4 for the onset of resin cracking. These voids take the form of bubbles entrapped in the fabric weave or in the surface layer of resin. Only one resin system was used, although both the resin system and the cure schedule are likely to influence resin cracking.

In the constant life diagram of Fig. 15 the hoop and axial stresses σ_x and σ_y are also σ_1 and σ_2 with $\sigma_6 = 0$. In spite of the large number of tests conducted and the fact that this diagram is cross-plotted from smoothed curves there is real difficulty in drawing smooth curves at all lives which appear mutually consistent and satisfy the assumed requirements of symmetry. This is particularly true for 10^6 cycles. It was found for chopped strand mat/polyester resin tubes [7] that the $R = 1$ condition was particularly damaging in fatigue, and there is a hint in Fig. 15 that this is true for the fabric reinforced tubes. It is assumed that this is due to the damaging stress perpendicular to the fibres acting equally on both sets of fibres. It is also known that a joint in chopped strand mat

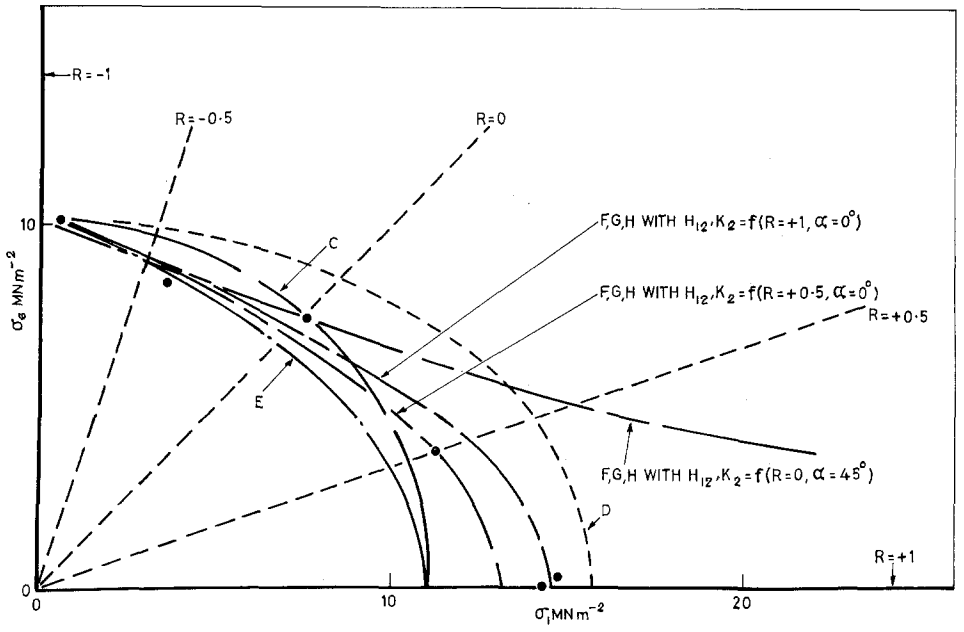

Figure 20 Fatigue results for the onset of damage in tubes at 10^6 cycles compared with the failure theories of Table I (see Table I for key to curves). R takes values from +1 to −1 with $\alpha = 45°$ corresponding to curve FB in Fig. 1.

reinforcement is significant both parallel and perpendicular to the damaging stress [2], thus the overlap may be doubly damaging at $R = +1.0$. Fig. 16 is also plotted in terms of hoop and axial stress σ_x and σ_y, but for a constant hoop stress σ_x, σ_1, σ_2 and σ_6 change for different values of R. In the static curve the assumed symmetry of shape shows that the observed result for $R = -1.0$ is premature and tends to confirm that the real in-plane shear strength ($-\sigma_1 = \sigma_2 = \sigma_6$ at this condition) should be about 110 MN m^{-2} as assumed previously.

The 10^6 cycle fatigue strengths are compared with failure theory predictions in Figs. 17 to 20. The comparisons with Group 2 theories are based on complex stress results for $R = +1.0$ and $\alpha = 0°$, $R = +0.5$ and $\alpha = 0°$ and $R = 0$ and $\alpha = 45°$ as before. The principal fatigue strengths are shown in Table III(b). F_{1t} ($= F_{2t}$) was taken as the hoop strength of $R = 0$, $\alpha = 0°$ tubes both for resin cracking and rupture. The principal compressive strengths F_{1c} ($= F_{2c}$) were based on the tensile strength using the ratio of tensile to compressive strength observed by Owen and Found [1] for flat laminates ($\alpha = 0°$). F_6 was taken from the $R = -1$, $\alpha = 45°$ tubes.

Figs. 17 and 18 show that for rupture Group 2 theories evaluated on $R = +1$, $\alpha = 0°$ data provide a useful conservative prediction of the observed results. In complete contrast evaluation from $R = 0$, $\alpha = 45°$ data produces an open-ended surface of no practical use. Evaluation from $R = 0.5$, $\alpha = 0°$ data appears to predict over-optimistic results for $R = 1.0$, $\alpha = 0°$. Of the simpler theories the Norris failure theory [13] provides reasonable predictions in the absence of complex stress data. Figs. 19 and 20 show that for resin cracking evaluation from $R = 0$, $\alpha = 45°$ data again leads to an unacceptable open-ended failure surface. Predictions based on $R = +1.0$, $\alpha = 0°$ and $R = +0.5$, $\alpha = 0°$ data are acceptable. None of the Group 1 theories provides agreement. The Norris failure theory is good if $\sigma_6 = 0$ (Fig. 19) but is unacceptable if $\sigma_6 \neq 0$ (Fig. 20).

8. General discussion and conclusions

This paper includes the results of 370 tests on tubes together with numerous results for flat specimens, and yet it was possible to explore only a limited part of the plane stress failure surfaces. In principle a failure surface should be uniquely determined from the principal strengths for simple theories together with the results of a single complex stress test for the more advanced theories. In practice a limited measure of agreement between predictions and results can only be obtained after highly subjective selection of data.

Previous workers have concluded that off-axis

flat specimens are inadequate and that filament-wound tubular specimens are to be preferred [23, 24]. It has previously been observed that the use of 45° off-axis specimens leads to open-ended and/or intersecting failure surfaces for the Group 2 failure theories [1]. Wu [5] and Tsai and Wu [7] have shown that failure surfaces predicted for such data are particularly sensitive to small changes in strength values. However the use of tubular specimens for prepared reinforcements such as mat, or fabric inevitably involves joints which cause great difficulty in the interpretation of results. These reinforcements account for a large proportion of the commercial market and the design significance of joints should not be missed. Notwithstanding the use of tubular specimens the present results show that it is still only too easy to obtain wildly varying predictions for other parts of the failure surface. The $R = 0$, $\alpha = 45°$ tube equivalent to the 45° off-axis flat specimen is just as bad as the flat specimen. On balance the $R = 1$, $\alpha = 0°$ condition seems to be the most reliable of those available with the present machine. None of the Group 1 theories was generally adequate although the Norris failure [13] theory was reasonable for both static and fatigue rupture.

There have been proposals to extend the tensor theories by the inclusion of cubic terms [25] thus increasing the number of normal stress interaction coefficients and permitting tension–tension and compression–compression interactions to be treated separately whilst retaining a continuous surface. From the practical and commercial point of view any proposal which requires more testing is unacceptable. Indeed the present work would be hopelessly uneconomic for most applications. In practice simpler theories are required, and this may involve separate evaluation for different regions of the failure surface. Failure theories do not pay any heed to damage mechanisms or failure modes. In practice these vary in different regions of the failure surface and it may well be that this produces discontinuous or intersecting failure surfaces.

Acknowledgement

This paper is based on results included in a Ph.D. thesis by J.R. Griffiths. The work was supported by a Science Research Council grant to M.J. Owen and by a research studentship awarded to J.R. Griffiths. The authors are indebted to Mr G. Budd for assistance in the preparation of specimens.

References

1. M. J. OWEN and M. S. FOUND, *J. Phys. D* **8** (1975) 480.
2. J. R. GRIFFITHS, Ph.D. Thesis, University of Nottingham (1974).
3. G. J. SCHNEIDER, *Fibre Sci. Tech.* **5** (1972) 29.
4. B. R. COLLINS and R. L. CRANE, *J. Composite Mater.* **5** (1971) 408.
5. E. M. WU, *ibid.* **6** (1972) 472.
6. M. J. OWEN and M. S. FOUND, Faraday Special Discussions of the Chemical Society, No. 2 (1972) 77.
7. M. J. OWEN, J. R. GRIFFITHS and M. S. FOUND, Proceedings of the 1975 International Conference on Composite Materials, Vol. 2 (Metals Society of the AIME, New York, 1976) pp. 917–941.
8. E. Z. STOWELL and T. S. LIU, *J. Mech. Phys. Solids* **9** (1961) 242.
9. M. E. WADDOUPS, General Dynamics Fort Worth Division, Report F2M 4763 (1967).
10. R. HILL, *Proc. Roy. Soc. A* **193** (1948) 281.
11. V. D. AZZI and S. W. TSAI, *Exptl. Mech.* **5** (1965) 283.
12. C. B. NORRIS and P. F. McKINNON, US Forest Products Lab. Report 1328 (1956).
13. *Idem,* US Forest Products Lab. Report 1816 (1962).
14. O. HOFFMAN, *J. Composite Mater.* **1** (1967) 200.
15. H. G. FRANKLIN, *Fibre Sci. Tech.* **1** (1968) 137–50.
16. I. I. GOLDENBLAT and V. A. KOPNOV, *Polymer Mech.* **1** (1965) 54.
17. S. W. TSAI and E. M. WU, *J. Composite Mater.* **5** (1971) 58.
18. E. K. ASHKENAZI, *Mekhanika Polimerov* **1** (1965) 79.
19. R. B. PIPES and B. W. COLE, *J. Composite Mater.* **7** (1973) 246.
20. M. J. OWEN, *J. Plast. Inst.* **35** (1967) 353.
21. M. S. FOUND, Ph.D. Thesis, University of Nottingham (1972).
22. M. J. OWEN, *Composites* **1** (1970) 346.
23. N. J. PAGANO and J. M. WHITNEY, *J. Composite Mater.* **4** (1970) 360.
24. J. J. LUCAS and J. B. SAINSBURY-CARTER, *J. Mater., JMLSA* **4** (1972) 586.
25. T. PRIDDY, *Trans. ASME* **96** (1974) 91.

Received 19 September and accepted 4 November 1977.